Power Quality Improvement in a PV Based EV Charging Station Interfaced with Three Phase Grid

ASSOCIATE PROFESSOR: ***Dr. M.ANITHA***

Y.SRAVANI[1], Sk.SADIF[2], Y.CHARAN[3], T.PAVAN

[1]STUDENT, [2]STUDENT, [3]STUDENT, [4]STUDENT

DEPARTMENT OF ELECTRICAL & ELECTRONICS ENGINEERING,

R.V.R & J.C. COLLEGE OF ENGINEERING, GUNTUR, ANDHRA PRADESH, INDIA.

ABSTRACT

This paper addresses enhancing power quality in a solar photovoltaic (PV) array-driven Electric Vehicle (EV) charging station. This station can function independently, utilizing PV array-generated power to charge EV batteries, while also interfacing with the utility grid to supply excess power. Additionally, it offers reactive power compensation to enhance grid power quality. The charging station serves several purposes: (i) compensating harmonic currents, (ii) controlling EV battery charging/discharging, (iii) simultaneous EV battery charging and harmonic current compensation, and (iv) simultaneous discharging and harmonic current compensation. The control system ensures the charging station operates effectively even under unbalanced grid voltages, reducing total harmonic distortion in grid currents to below 5% as per IEEE-519 standards. It is designed to primarily function in grid-connected mode. However, if synchronism with the grid is lost, it seamlessly transitions to standalone mode, with the PV array charging the EV battery. Additionally, a synchronization control mechanism is developed to reconnect the system to the grid when it becomes available.

I. INTRODUCTION:

Increasing environmental concerns, such as pollution and resource conservation, have driven the widespread adoption of electric vehicles (EVs) [1]. This surge in EV demand necessitates the installation of charging stations. Traditionally, EV batteries are charged using power from the grid, as depicted in charger topologies outlined in [2-4]. However, these topologies heavily rely on grid power for charging, leading to unidirectional power flow, which restricts the flow of active power from the vehicle to the grid. Nonetheless, EV batteries can serve as energy storage to supply power during peak demand [5]. Often, EVs are parked with ample stored energy, which can be supplied to the grid when the vehicle is idle, effectively addressing peak power requirements. To achieve this, EV chargers must support bidirectional active power flow [6], a process referred to as vehicle-to-grid (V2G). In V2G mode, EV chargers can also provide reactive power support to the grid [7-10], typically near the load end [9].

The intermittency of photovoltaic (PV) power generation can be mitigated by utilizing EV batteries as buffer storage and integrating charging stations with the grid [10]. While onboard chargers have been demonstrated [11], they are more suitable for low-powered batteries, making off-board chargers a preferable solution [12-13]. This paper presents a single-stage PV-based off-board EV charging station connected to the grid, facilitating bidirectional power flow. The EV connects to the charging station's DC-link via a bidirectional converter, which blocks second harmonic currents and DC-link ripples from affecting the EV battery, thus enhancing battery lifespan. Additionally, the dependence of EV battery rating selection on DC-link voltage is eliminated. The duty cycle of the bidirectional converter controls battery charging/discharging.

The PV array charges the EV battery and supplies excess power to the utility, reducing generation requirements. A voltage source converter (VSC) is employed for reactive power compensation as demanded by the grid, thereby enhancing grid power quality in grid-connected mode. During grid failure, the system operates in standalone mode, utilizing PV array generation for EV battery charging. The system undergoes testing under various dynamic conditions, including PV insolation variations, grid voltage imbalances, and reactive power compensation. Upon grid restoration, the charging station synchronizes with the grid.

The charging station's control is designed based on reference active power and reactive power commands. The EV owner determines the active power command for charging/discharging the EV battery, while the reference reactive power is selected based on inductive/capacitive reactive power requirements for continuous charging station

operation. The charging station enables EV owners to control EV battery charging/discharging, with grid-to-vehicle (G2V) operation for charging from the grid and vehicle-to-grid (V2G) operation for discharging to the grid. Moreover, the station provides reactive power compensation (lagging/leading) as required.

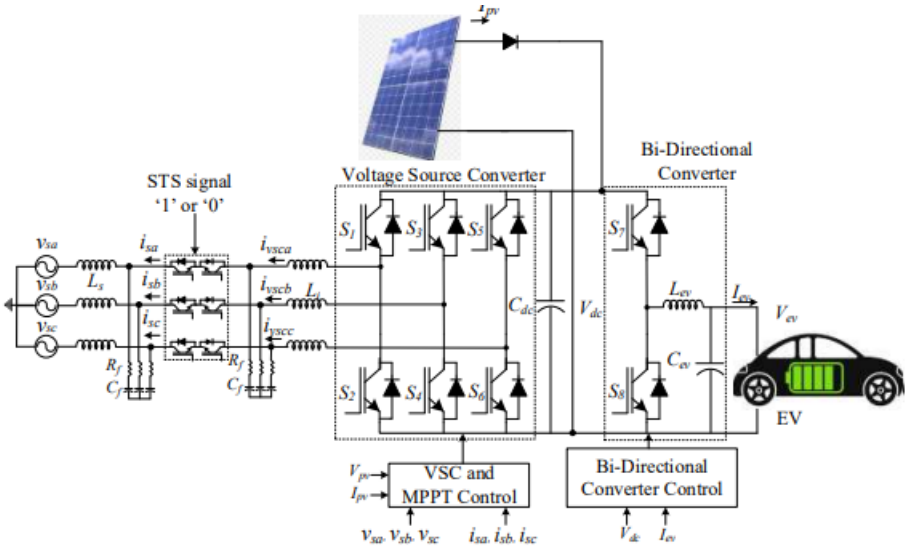

Fig. 1 Three-phase Three wire single-stage grid connected PV system with EV

II SYSTEM CONFIGURATION:

The basic block diagram of the single-stage PV-based EV charging station is illustrated in Figure 1. The primary objective of this charging station is to charge the electric vehicle (EV) battery using the direct current (DC) power generated by the photovoltaic (PV) array. A bi-directional converter is employed to manage the charging and discharging of the EV battery. This converter allows for bidirectional flow of power, enabling energy to be transferred both from the PV array to the battery for charging and from the battery to other loads when discharging.

In this setup, the PV array is directly connected to the DC-link of the system. This means that there is no need for an intermediate boost converter, which is typically used to raise the voltage of the PV array output to match the battery voltage. By eliminating the boost converter, the overall cost of the charging station is reduced, and efficiency is potentially increased since fewer conversion stages are involved.

To interface the DC power from the PV array and battery with the grid, an Insulated Gate Bipolar Transistor (IGBT) based Voltage Source Converter (VSC) is utilized. This VSC is responsible for converting the DC power to alternating current (AC) power, which can then be fed into the grid. Additionally, IGBT-based switches, known as Static Transfer Switches (STS), are employed to connect the charging station with the grid. These switches enable seamless transition between grid-connected and standalone operation modes, ensuring uninterrupted power supply to the EV battery.

In summary, the single-stage PV-based EV charging station simplifies the charging process by directly utilizing PV-generated DC power to charge the EV battery. The integration of a bi-directional converter eliminates the need for a boost converter, reducing costs and potentially improving efficiency. The VSC and STS facilitate the conversion and connection of DC power to the grid, ensuring efficient and reliable operation of the charging station.

III CONTROL SCHEME:

The primary objective of the present charging station is to effectively utilize PV array generation in EV charging, while also being synchronized to the grid to allow the PV array power to be supplied to the grid. Additionally, the EV has the capability to discharge and supply power to the grid. Therefore, an intelligent control scheme is crucial for optimizing the charging station's performance. The control approach, demonstrated in Figure 2, is based on two input commands:

3.1. Active Power Reference Command:

This command is determined based on whether the EV battery needs to be charged or discharged. The decision is made by the EV owner, depending on their preference to either charge the EV battery or discharge it to supply power to the grid, thus earning incentives b The in-phase UTs are estimated as, The in-phase UTs are estimated as, The in-phase UTs are estimated as, The in-phase UTs are estimated as, The in-phase UTs are estimated as, The in-phase UTs are estimated as, The in-phase UTs are estimated as, The in-phase UTs are estimated as, The in-phase UTs are estimated as, The in-phase UTs are estimated as, y selling power during peak demand.

3.2 Reactive Power Reference Command:

This command governs both the amount and the nature (inductive or capacitive) of reactive power required. The control of the EV charging station is divided into two subsections: VSC control and EV charging/discharging control, in both grid-connected and standalone modes. In the VSC control during grid-connected mode, the active power reference command contributes to the generation of switching pulses for the VSC, enabling efficient management of power flow between the PV array, EV battery, and the grid. The EV battery charging/discharging is controlled using a bidirectional DC-DC converter.

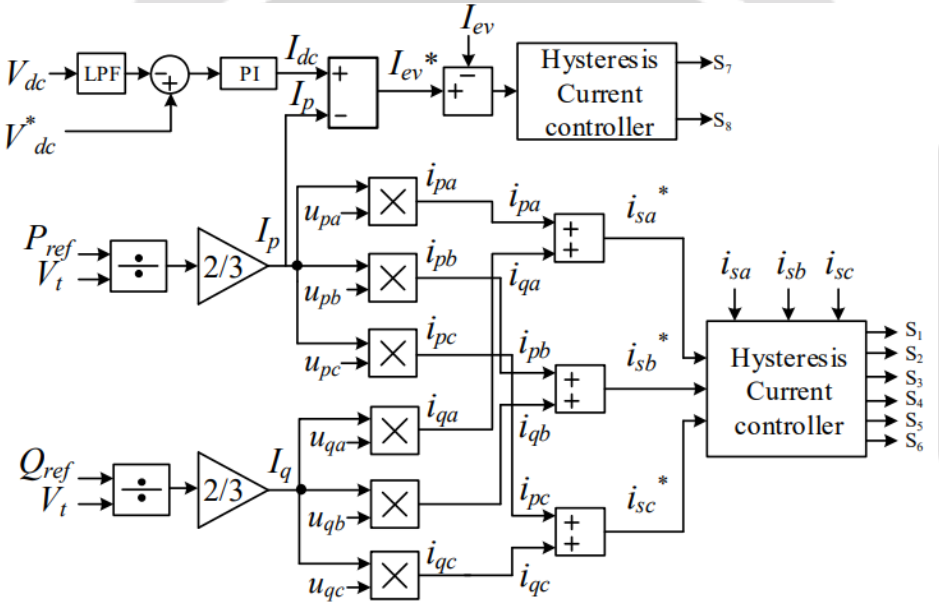

Fig. 2 Controller diagram

Further details regarding the control scheme will be provided in the subsequent sections, outlining the control strategies for both grid-connected and standalone modes, ensuring the efficient and effective operation of the charging station.

3.3 VSC Control in Grid Connected Mode

In the grid-connected mode, the generation of gate pulses for the Voltage Source Converter (VSC) is demonstrated in Figure 2. The Active Power Reference Command (P_{ref}) contributes to the active component of the current (I_p), while the Reactive Power Reference Command (Q_{ref}) contributes to the reactive component of the current (I_q). The per-phase active currents (i_{pa}, i_{pb}, i_{pc}) are estimated by multiplying the active component of the current (I_p) with the in-phase unit templates (u_{pa}, u_{pb}, u_{pc}). Similarly, the per-phase reactive currents (i_{pa}, i_{pb}, i_{pc}) are estimated by multiplying the reactive component of the current (I_q) with the quadrature-phase unit templates (u_{pa}, u_{pb}, u_{pc}). These estimations form the basis for controlling the VSC in the grid-connected mode.

3.3.1 Estimation of In-phase and Quadrature-phase Unit Templates (UTs) and Amplitude of the Terminal Voltage:

When the grid voltages are unbalanced, their Positive Sequence Components (PSCs) are estimated, as illustrated in Fig. 3. The terminal voltage amplitude is then estimated from the PSCs using the following procedure:

$$\sqrt{\frac{2}{3}(v_{pa}^2 + v_{pb}^2 + p_{pc}^2)}$$

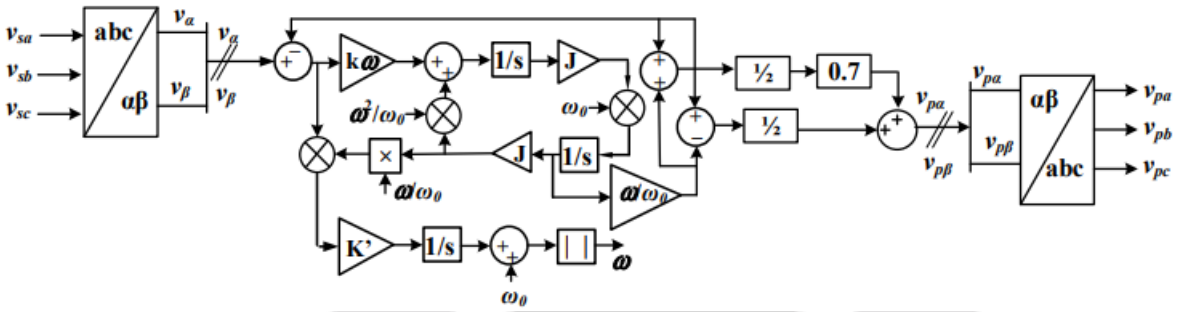

Fig.3 Positive sequence grid voltages estimation

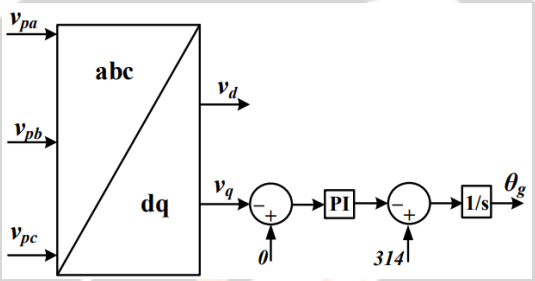

Fig.4 Estimation of grid voltage phase angle

The in-phase UTs are estimated as,

$$u_{pa} = \frac{v_{pa}}{V_t}, u_{pb} = \frac{v_{pb}}{V_t}, u_{pc} = \frac{v_{pc}}{V_t}$$

Similarly, the quadrature phase UTs are computed as,

$$u_{qa} = -\frac{u_{pa}}{\sqrt{3}} + \frac{u_{pc}}{\sqrt{3}}, u_{qb} = -\frac{\sqrt{3}u_{pa}}{2} + \frac{(u_{pb}-u_{pc})}{2\sqrt{3}}, u_{qb} = -\frac{\sqrt{3}u_{pa}}{2} + \frac{(u_{pb}-u_{pc})}{2\sqrt{3}}$$

The in-phase and quadrature-phase Unit Templates (UTs) obtained in steps (2) and (3) are utilized to estimate the reference grid currents. In Fig. 4, the estimation of the grid voltage phase angle is demonstrated. This phase angle information is crucial for accurately estimating the reference grid currents. The gate pulses for the Voltage Source Converter (VSC) are generated by subtracting the reference grid currents (i_{sa}^*, i_{sb}^* and i_{sc}^*) from the sensed grid currents (i_{sa}, i_{sb}, and i_{sc}), which are synchronized with the grid phase. These calculated differences are then fed into hysteresis current comparators v_{sa}, v_{sb}, and v_{sc}), which generate the gate pulses for controlling the VSC.

3.3.2 Grid Currents Active Component Estimation

The grid current's active and reactive components play a crucial role in determining the amplitude of the grid reference currents and the phase difference between grid voltages and grid currents. The active component of the grid current, denoted as Ip, represents the active power flowing into the charging station. This component can be estimated by using the active power reference command (P_{ref}) and the terminal voltage amplitude.

$$I_p = \frac{2}{3} * \frac{P_{ref}}{V_t}$$

If grid current active component (I_p) is positive, then EV battery charges else if I_p is negative, EV battery discharges.

3.3.3 Grid Currents Reactive Component Estimation

The grid current reactive component (I_q) signifies the reactive power exchange. It is estimated using reactive power reference command ((Q_{ref}) and terminal voltage amplitude as

$$I_p = \frac{2}{3} * \frac{P_{ref}}{V_t}$$

3.3.4 Grid Reference Currents Computation

The active component of the grid current (I_p) and reactive component of the grid current (I_q) are used for the estimation of the in-phase and the quadrature phase components of the reference grid currents. These components are used for calculation of the grid reference currents as,

$$i_{sa}^* = i_{pa} + i_{qa}, i_{sb}^* = i_{pb} + i_{qb}, i_{sc}^* = i_{pc} + i_{qc}$$

where, i_{pa}, i_{pb}, i_{pc} and i_{qa}, i_{qb}, $i_{qc}$are in-phase components of the reference grid currents and quadrature components of the reference grid currents. These components are calculated as,

$$i_{pa} = I_p \times u_{pa}, i_{pb} = I_p \times u_{pb}, i_{pc} = I_p \times u_{pc}$$

$$i_{qa} = I_q \times u_{qa}, i_{qb} = I_q \times u_{qb}, i_{qc} = I_q \times u_{qc}$$

The gate pulses for the VSC are generated by deducting reference grid currents (i_{sa}^*, i_{sb}^* and i_{sc}^*) from sensed grid currents (i_{sa}, i_{sb}, i_{sc}) and feeding them to hysteresis current controller.

3.4 Standalone Mode and Synchronization Control

During the grid failure, the changing station shifts to standalone mode. The grid voltage and PCC voltage phase angles (θ_g and θ_s) are compared and the error is evaluated as,

$$\theta_e(k) = \theta_g(k) - \theta_s(k)$$

where θ_g is calculated as shown in Fig. 4.

This error is provided to the PI controller to obtain the frequency error as,

$$\Delta\theta_d(k) = \Delta\theta_d(k-1) + k_{ps}\{\theta_e(k) - \theta_e(k-1)\} + k_{is}\{\theta_e(k)\}$$

where, k_{ps} and k_{is} are PI controller gains coefficients.

The new phase angle θ_n is estimated as,

$$\theta_n(k) = \theta_s(k) + \Delta\theta_d(k)$$

When operating in standalone mode, VSC generates the sinusoidal reference voltages from the peak amplitude of phase voltage (V_{ts}) at PCC as,

$$v_{vsca}^* = V_{ts}\sin(\theta_n)$$

$$v_{vscb}^* = V_{ts}\sin(\theta_n - 120)$$

$$v_{vscc}^* = V_{ts}\sin(\theta_n - 240)$$

where, θ_n is the phase reference angle and V_{ts} =230∗√2/(√3 V). It is evaluated by integration of the reference angular frequency. After that sensed phase voltages are compared to the reference voltages obtained in (1) and the voltage errors (v_{ea}, v_{eb}, v_{ec}) obtained are provided to the PI controller.

$$i^*_{vsca} = i^*_{vsca}(k-1) + k_{pv}\{v_{ea}(k) - v_{ea}(k-1)\} + k_{iv}\{v_{ea}(k)\}$$

$$i^*_{vscb} = i^*_{vscb}(k-1) + k_{pv}\{v_{eb}(k) - v_{eb}(k-1)\} + k_{iv}\{v_{eb}(k)\}$$

$$i^*_{vscc} = i^*_{vscc}(k-1) + k_{pv}\{v_{ec}(k) - v_{ec}(k-1)\} + k_{iv}\{v_{ecv}(k)\}$$

The reference currents obtained are compared with the sensed PCC currents and is provided to the hysteresis current controller to generate the switching pulses of the VSC

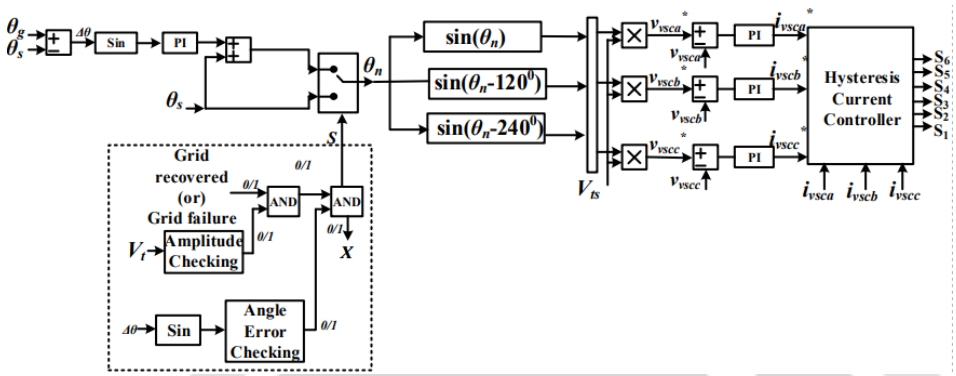

Fig. 5 Synchronization control

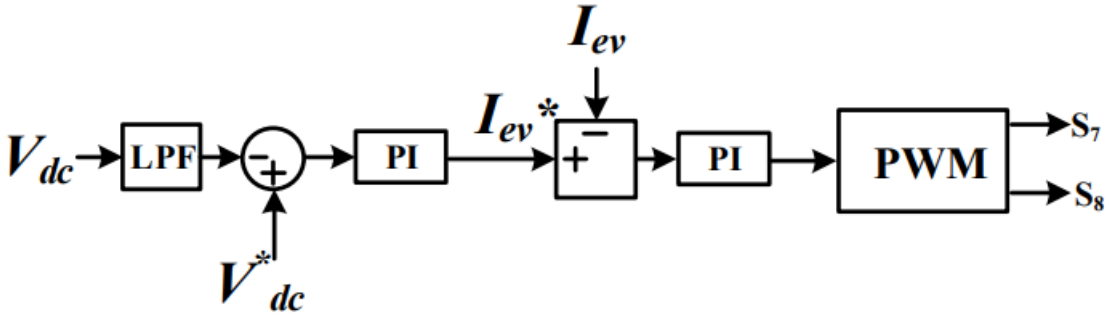

Fig. 6 EV charging/discharging control in standalone mode

When restoring the grid from islanded status, the control synchronizes grid voltages (vs) with PCC voltages (v^*_{vscc}) prior to connection. Illustrated in Fig. 5, the synchronization control relies on parameters like grid voltage amplitude (V_t), phase angle (θ_e), and grid frequency (fs) to determine system operating mode. If V_t exceeds 1.1pu or falls below 0.88pu, if $\theta_g \neq \theta_s$, or if fs exceeds 50.5Hz or drops below 49.5Hz, the system is deemed abnormal and transitions to islanding mode. Based on these voltage and frequency conditions, the synchronization control signals '1' (on) or '0' (off) to STS (Static Transfer Switches), determining whether the system operates in grid-connected or islanding mode.

3.5 EV Charging/Discharging Control in Standalone Mode

In standalone mode, the controller utilizes MPPT to derive the reference DC-link voltage (V^*_{dc}), ensuring stability amid dynamic conditions. Designed to maintain a constant DC-link voltage, the controller orchestrates EV charging/discharging operations without disruption. A consistent power exchange with the grid is upheld to prevent any undue strain on the grid.

$$I^*_{ev} = I_{dc} + I_p$$

Where I_{dc} regulates the DC-link voltage to V^*_{dc}. This I_{dc} is calculated by passing the error, obtained by subtracting the sensed DC-link voltage from V^*_{dc}, through a PI controller as follows:

$$I_{ev}^{*} = \left(k_{pd} + {}^{k_{id}}/_{s}\right)\{V_{dc}^{*} - V_{dc}\}$$

The battery reference current (I_{ev}^{*}) is then compared with the EV current and fed into the PI controller to produce gating pulses for the bidirectional converter, as depicted in Figure 6.

IV RESULTS AND DISCUSSION:

A laboratory prototype of a single-stage PV-based EV charging station connected to a 3-phase grid has been developed. The performance of the charging station under various steady-state and dynamic conditions is detailed in the following sections.

4.1 Response of Charging Station at Steady State

In Fig. 7(a), the three-phase grid voltages are measured at 213.37 V, 216.99 V, and 214.70 V, while the corresponding grid currents are 4.987 A, 5.155 A, and 5.072 A, respectively. These readings indicate well-balanced and sinusoidal grid currents. The power factor is close to unity, approximately 0.9978, as shown in Fig. 7(b). Additionally, Fig. 7(b) illustrates the power delivered to the grid by the PV array, measured at 1.885 kW. The total harmonic distortions (THDs) of the grid voltages and currents are within acceptable limits, measured at 2.02%, 2.09%, 2.07% and 3.36%, 3.10%, 3.32%, respectively, as depicted in Figs. 7(c-d). Fig. 7(e) presents the grid voltages and currents unbalancing factor, measured at 0.98% and 1.41%, respectively. In Figs. 7(f-g), the EV voltage, current, and power consumed by the EV are displayed as 289.1 V, 5.139 A, and 1.68 kW, respectively. The negative sign associated with the grid power and EV power indicates power consumption. Furthermore, the PV array generates a power of 3.79 W, as shown in Fig. 7(h).

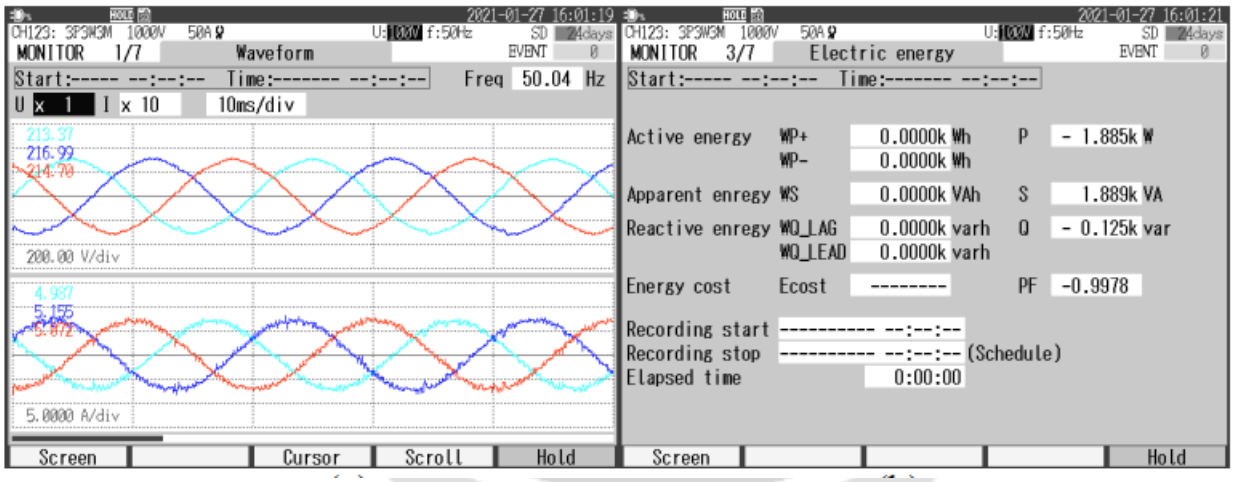

(a) (b)

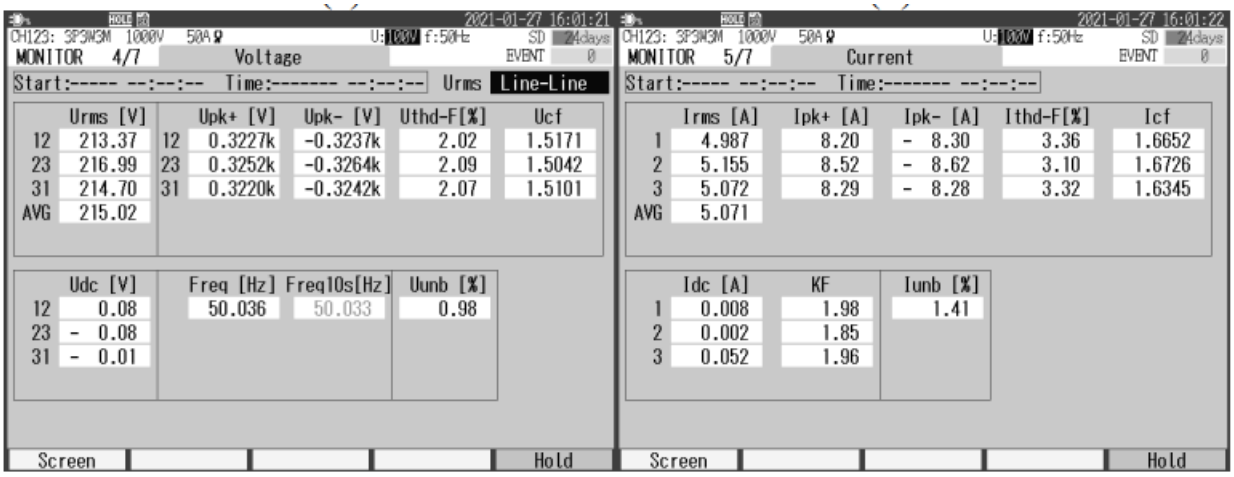

(c) (d)

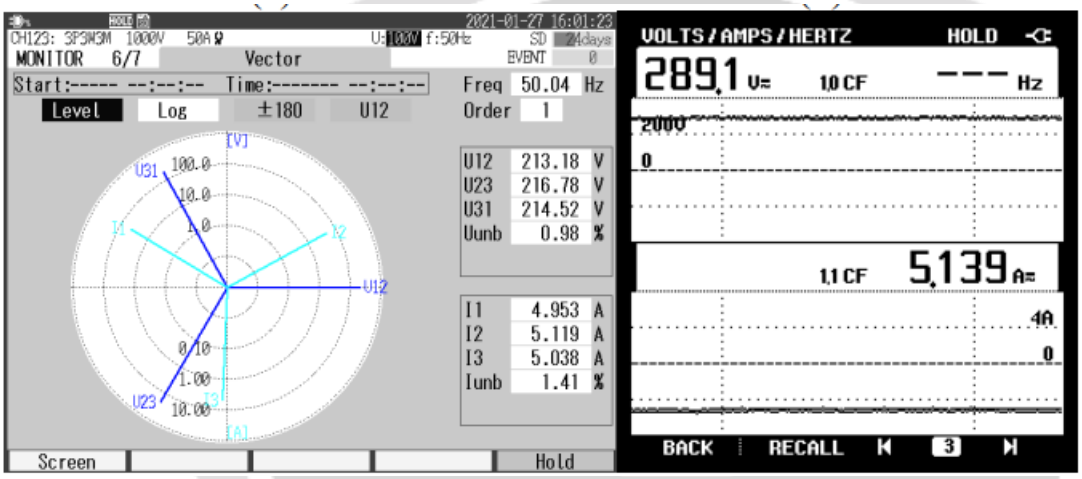

(e) (f)

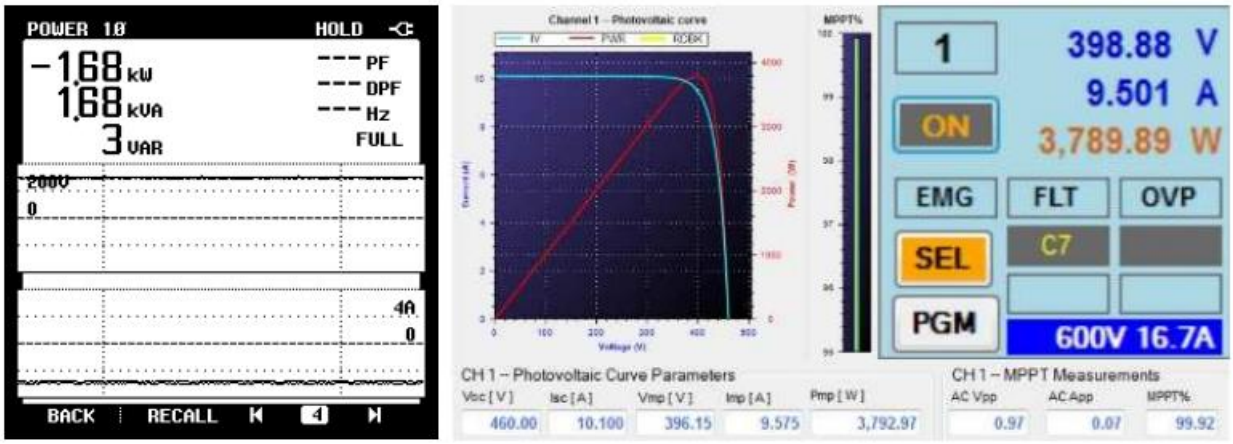

(g) (h)

Fig. 7 Charging Station at Steady State (a-b) v_{sab} and i_{sa} (c) P_s (d) Harmonics spectra of v_{sab} (e) Harmonics spectra of i_{sa} (f) phasor diagram of vsab and i_{sa} (g) PV power (h) v_{ev} and i_{ev} (i) P_{ev}

4.2 Dynamic Performance of Charging Station

In Fig. 8(a), the charging station's response to a decrease in PV insolation is depicted. As the PV insolation decreases, power production diminishes, leading to a decline in PV array current. Since the EV is charging at a constant rate, the reduction in energy production is compensated by the grid, resulting in a decrease in grid current without any alteration in PV voltage, DC-link voltage, or EV current.

Fig. 8(b) illustrates the charging station's performance during an increase in PV insolation. With a rise in PV insolation, the PV array current increases, resulting in greater power production. If the EV is charging at a constant rate, the surplus power generated is fed back to the grid. However, the PV voltage and DC-link voltage remain constant, with no change in EV current. In the scenario where the grid operates in constant power mode, an increase in PV insolation prompts the EV to consume the additional power, resulting in a faster charging rate, as depicted in Fig. 8(c). Consequently, VSC current and grid current remain unaffected, as the VSC supplies a constant current to the grid, while the rate of EV charging escalates.

In the event of a rise in PV insolation causing simultaneous grid voltage imbalance, the grid compensates for the extra power, resulting in an increase in grid currents. Despite this, the grid currents maintain balance and sinusoidal waveform, even when the grid voltages exhibit significant imbalance.

4.3 Charging Station Performance during Reactive Power Compensation to Grid

In accordance with the control scheme outlined in Fig. 2, the charging station can supply reactive power compensation to the grid upon demand. To validate this capability, a reference reactive power of -1 KVAR is applied to the controller. As depicted in Fig. 9(a), when capacitive reactive power is required, the charging station delivers it successfully, evidenced by the grid current leading the grid voltage. Conversely, when suddenly instructed to provide inductive reactive power, the direction of the grid current reverses, with the grid current lagging behind the grid voltage, indicating provision of inductive reactive power. Throughout this transition, the DC-link voltage and PCC voltage remain stable. Fig. 9(b) illustrates the reactive power transition from 1 KVAR to -1 KVAR. Initially, the grid current lags the grid voltage, but after the transition, it leads the grid voltage. Thus, the EV charging station demonstrates its capability to supply both capacitive and inductive reactive power as needed, while ensuring the stability of PCC voltage and the DC-link voltage.

4.4 Performance during Synchronization

The performance of the charging station during grid disconnection, reconnection, and synchronization is illustrated in Figs. 10(a-c). Initially, the station operates in grid-connected mode, but when the grid disconnects, both the grid current and θ_g promptly drop to zero. However, the PV array continues to generate power. During this period, the station can switch to standalone mode, ensuring uninterrupted operation. Furthermore, the station can compensate for reactive power when connected to the grid, demonstrating its versatility. Experimental tests confirm satisfactory operation in both grid-connected and standalone modes. The charging station synchronizes with the grid when available, enabling it to feed excess power back to the grid. Experimental results validate the station's performance under dynamic conditions such as PV insolation variations, grid voltage imbalance, and reactive power compensation.

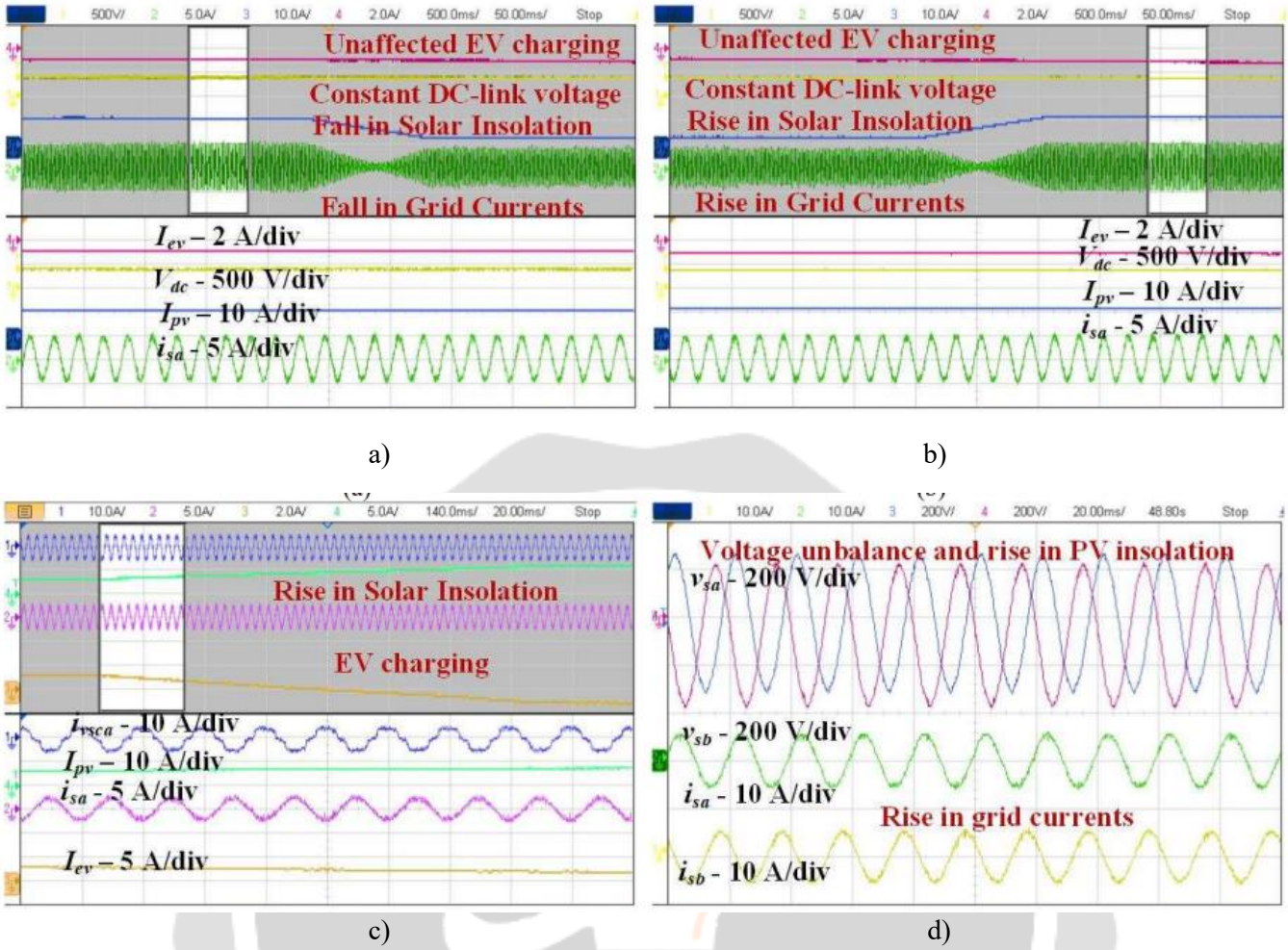

Fig. 8 Dynamic response of grid connected system at (a) Increase in solar insolation (b) Fall in PV insolation (c) voltage unbalance and rise in PV insolation

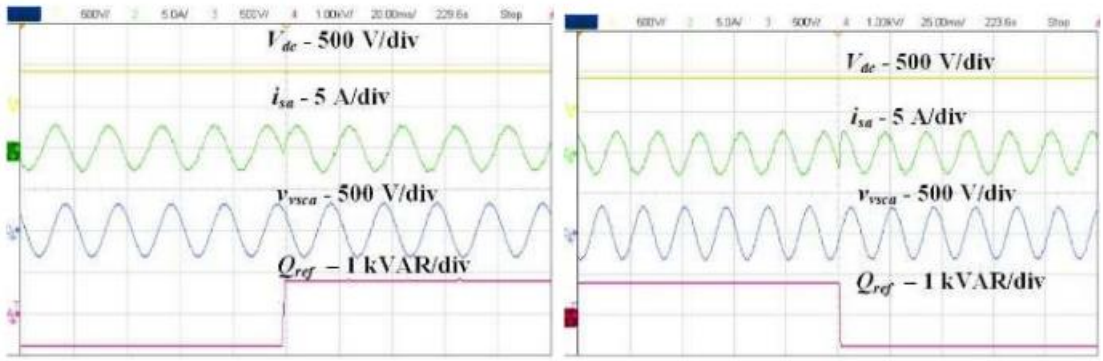

Fig. 9 Charging station providing reactive power compensation to the grid

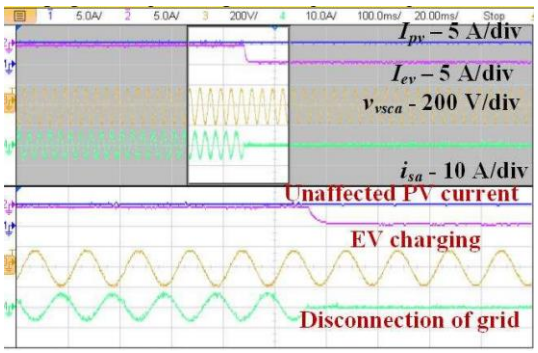

a)

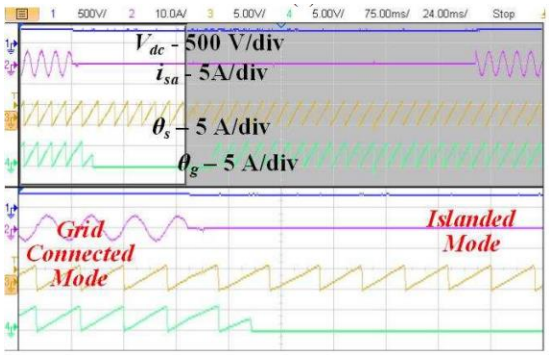

b)

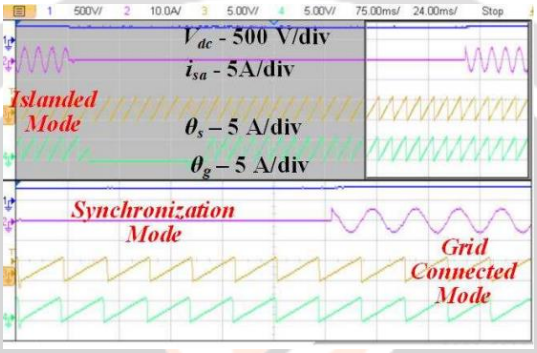

c)

Fig. 10 Performance during synchronization

V CONCLUSION:

A single-stage photovoltaic (PV) based electric vehicle (EV) charging station has been designed to synchronize with the grid and feed power generated by the station back to the grid. This design aims to earn profits by selling excess power and by discharging EV batteries to the grid during peak hours. The charging station can also compensate for reactive power when connected to the grid.

Testing has shown that the charging station operates satisfactorily in both grid-connected and standalone modes. It synchronizes with the grid when available and feeds excess power back to the grid. Experimental results have validated the station's performance under dynamic conditions such as varying PV insolation, unbalanced grid voltages, and reactive power compensation.

APPENDICES

Solar PV array: Open circuit voltage (V_{oc}) =460V, Short circuit current (I_{sc}) = 10.1A, EV battery: 240V, 14Ah (Lead Acid), J = [0 -1; 1 0].

REFERENCES

[1] M. Shatnawi, K. B. Ari, K. Alshamsi, M. Alhammadi and O. Alamoodi, “Solar EV charging,” in Proc. 6th Inter. Conf. on Renewable Energy: Generation and Applications (ICREGA), 2021, pp. 178-183.

[2] P. P. Nachankar, H. M. Suryawanshi, P. Chaturvedi, D. D. Atkar, C. L. Narayana and D. Govind, “Universal off-board battery charger for light and heavy electric vehicles,” in Proc. IEEE Inter. Conf. on Power Elect., Drives and Energy Systems (PEDES), 2020, pp. 1-6.

[3] P. K. Sahoo, A. Pattanaik, A. K. Dey and T. K. Mohapatra, “A novel circuit for battery charging and motor

control of electric vehicle," in Proc.1st Odisha Inter. Conf. on Electrical Power Engineering, Communication and Comp.Technology (ODICON), 2021, pp.1-6.

[4] P. Rehlaender, F. Schafmeister and J. Böcker, "Interleaved single- stage LLC converter design utilizing half- and full-bridge configurations for wide voltage transfer ratio applications," IEEE Transactions Power Electronics, vol. 36, no. 9, pp. 10065-10080, Sept. 2021.

[5] B. B. Quispe, G. de A. e Melo, R. Cardim and J. M. de S. Ribeiro, "Single-phase bidirectional PEV charger for V2G operation with coupled-inductor Cuk converter," in Proc. 22nd IEEE International Conference on Industrial Technology (ICIT), 2021, pp. 637-642.

[6] H. Heydari-doostabad and T. M. O'Donnell, "A wide range high voltage gain bidirectional DC-DC converter for V2G and G2V hybrid EV charger," IEEE Transactions Industrial Electronics, Early Access.

[7] C. Tan, Q. Chen, L. Zhang and K. Zhou, "Frequency adaptive repetitive control for three-phase four-leg V2G inverters," IEEE Transactions Transportation Electrification, Early Access.

[8] K. Lai and L. Zhang, "Sizing and siting of energy storage systems in a military-based vehicle-to-grid microgrid," IEEE Transactions Industry Applications, vol. 57, no. 3, pp. 1909-1919, May-June 2021.

[9] M. H. Mehraban Jahromi, P. Dehghanian, M. R. Mousavi Khademi and M. Z. Jahromi, "Reactive power compensation and power loss reduction using optimal capacitor placement," in Proc. IEEE Texas Power and Energy Conference (TPEC), 2021, pp. 1-6.

[10] M. J. Aparicio and S. Grijalva, "Economic assessment of V2B and V2G for an office building," in Proc. 52nd North American Power Symposium (NAPS), 2021, pp. 1-6.

[11] A. S. Daniel and K. R. M. V. Chandrakala, "Design of an isolated onboard plug-in electric vehicle charger," in Proc. 7th International Conf. on Electrical Energy Systems (ICEES), 2021, pp. 147-149.

[12] H. Rasool et al., "Design optimization and electro-thermal modeling of an off-board charging system for electric bus applications," IEEE Access, vol. 9, pp. 84501-84519, 2021.

[13] S. Koushik and V. Sandeep, "Design and selection of solar powered off-board domestic charging station for electric vehicles," in Proc. International Conference on Sustainable Energy and Future Electric Transportation (SEFET), 2021, pp. 1-6.

[14] X. He, H. Geng and G. Yang, "A generalized design framework of notch filter based frequency-locked loop for three-phase grid voltage," IEEE Transactions Industrial Electronics, vol. 65, no. 9, pp. 7072- 7084, Sept. 2018.